Clim Dyn (2007) 28:581–597
DOI 10.1007/s00382-006-0202-0

Parameterisation of orographic cloud dynamics in a GCM

S. M. Dean · J. Flowerdew · B. N. Lawrence · S. D. Eckermann

Received: 20 March 2006 / Accepted: 6 October 2006 / Published online: 8 December 2006

Abstract A new parameterisation is described that predicts the temperature perturbations due to sub-grid scale orographic gravity waves in the atmosphere of the 19 level HadAM3 version of the United Kingdom Met Office Unified Model. The explicit calculation of the wave phase allows the sign of the temperature perturbation to be predicted. The scheme is used to create orographic clouds, including cirrus, that were previously absent in model simulations. A novel approach to the validation of this parameterisation makes use of both satellite observations of a case study, and a simulation in which the Unified Model is nudged towards ERA-40 assimilated winds, temperatures and humidities. It is demonstrated that this approach offers a feasible way of introducing large scale orographic cirrus clouds into GCMs.

S. M. Dean (✉)
National Institute of Water and Atmospheric Research Ltd, Wellington, New Zealand
e-mail: s.dean@niwa.co.nz

J. Flowerdew
Atmospheric Oceanic and Planetary Physics, Clarendon Laboratory, University of Oxford, Oxford, Oxfordshire, UK

B. N. Lawrence
British Atmospheric Data Centre, Rutherford Appleton Laboratory, Chilton, Oxfordshire, UK

S. D. Eckermann
E. O. Hulburt Center for Space Research, Code 7646, Naval Research Laboratory, Washington, DC, USA

1 Introduction

In a recent paper, Dean et al. (2005) identified that cirrus, generated by orographic gravity waves over many mountain ranges, was an important cloud process that was missing in at least one GCM, the HadAM3 version of the United Kingdom Met Office atmospheric climate model, henceforth referred to here as the Unified Model. It was proposed that this deficiency existed because, in common with many models, scales smaller than the horizontal grid-box scale (typically of order one hundred to many hundreds of kilometres) are omitted, and that as a result a large part of the gravity wave spectrum is absent. It was believed that these missing gravity waves were responsible for generating cooling in the upper troposphere that could lead to the existence of large scale cirrus clouds. Similar deficiencies of continental cirrus have been identified by Fowler and Randall (1999).

Here we propose utilising a new sub-grid gravity wave parameterisation, based on existing GCM gravity wave drag schemes (Palmer et al. 1986; McFarlane 1987) that is capable of predicting the grid box average temperature perturbations that occur in the troposphere due to sub-grid scale gravity waves. This temperature perturbation can then be used in the cloud parameterisation in the model to generate orographic clouds, including cirrus. The scheme is implemented independently of the existing sub-grid gravity wave scheme and should thus be compatible with other models (e.g. the ''new dynamics'' version of the Unified Model).

There have been previous studies which have utilised gravity wave parameterisations to calculate sub-grid temperature perturbations. For example, Carslaw

et al. (1999), predicted the temperature perturbations in the lower stratosphere which can influence polar stratospheric clouds (PSCs): see also Höpfner et al. (2005) and Mann et al. (2005). Butchart and Knight (1999) used the existing gravity wave scheme in the Unified Model to calculate the magnitude of temperature perturbation from the wave stress at each level. Once again the interest was in the polar stratosphere and potential areas for the formation of PSCs. The work of Cusack et al. (1999) notes that the sub-grid probability distribution function used in the Unified Model cloud scheme attempts to compensate for the effects of unresolved gravity waves on the model clouds. Wilson and Gregory (2003) highlight the inadequacies of such an approach and similar ones such as that of Xu and Randall (1996). These approaches have not simulated the phase of the orographic gravity waves and thus whether they act to cool or warm the atmosphere locally. In the troposphere this is critical to the correct simulation of orographic clouds.

Nilson et al. (2000) used a Lagrangian aerosol box model to show that atmospheric waves can enhance the aerosol particle nucleation rates by up to five orders of magnitude due to the strong temperature fluctuations. They recommended that this effect should be included in climate model simulations. Similarly Karcher and Lohmann (2002) used a box model to show that large vertical velocities have a significant influence on cirrus nucleation. They suggest that incorporation of unresolved vertical velocities from all types of waves is required in GCMs to simulate the correct nucleation of cirrus. Lohmann et al. (1999) incorporated the effect of unresolved vertical velocities on the nucleation rate of cloud droplets by adding a term to the resolved vertical velocity that was a function of the turbulent kinetic energy. However, this approach assumes that unresolved velocities are dominated by the turbulent motions and is unable to create the geographical variations in cloud seen in observations. The orographic cloud scheme to be described in this paper is unique in that it explicitly calculates the sign of temperature perturbations by resolving the expected phase of sub-grid orographic gravity waves in the troposphere. This allows the scheme to realistically increase and decrease cloud in the troposphere.

We begin by describing in some detail the theory of the new parameterisation, including the explicit calculation of the phase. A case study over the Andes is used to demonstrate the ability of the scheme to simulate reasonable temperature perturbations when compared to a high resolution two dimensional model. A second case study is employed to evaluate the parameterisation's ability to simulate an orographic cloud event within the Unified Model. Observations from the International Satellite Cloud Climatology Project (ISCCP) and the Global Retrieval of ATSR-2 Cloud Parameters and Evaluation (GRAPE) project are used to identify and describe an orographic cloud over the South Island of New Zealand on the 1 July 1999. While the minimum requirement of a parameterisation is that it can reproduce the current climatological mean state, confidence in any predictions of future climate behaviour requires confidence in a parameterisation's ability to simulate actual meteorological events or regimes correctly. Reasonable representation of the underlying physics, rather than strong dependence on statistical methods, ensures that any change in the frequency of dynamical regimes or events will be reflected in the correct response of the parameterisation. As such we also present a method for analysing climate model parameterisations which can be used for evaluating performance in specific regimes or events.

2 New gravity wave scheme

Any gravity wave scheme first requires an estimate of an initial wave amplitude (or stress) which is dependent on the unresolved orography and the low level winds and stability. The wave generated can then be allowed to propagate vertically through a vertical column of atmosphere within a given horizontal grid box. In the simple case of a linear hydrostatic approximation the amplitude of the wave will tend to grow as the density of the atmosphere decreases, though this may be suppressed by changes in stability and windspeed. Additionally, this growth can be damped by wave saturation (breaking) mechanisms. For a parameterization where the vertical displacement of air is needed to influence cloud amounts, the phase of the wave must also be simulated at every level. Each of these calculations will now be explored in detail.

2.1 Surface amplitude

For the new gravity wave scheme it is necessary to calculate an initial wave amplitude at the surface rather than the usual stress. In general the average valley to peak height of sub-grid orography is taken to be $2\sigma^{1/2}$,where σ is the variance of all the sub-grid orography about the gridbox mean height. This would be a natural first guess for the surface vertical displacement amplitude of the wave (henceforth referred to as the surface wave amplitude). However, because orography

preferentially aligns as ridges, simply using this total variance would greatly underestimate or overestimate the true surface wave amplitude (depending on the surface wind direction). It is more useful to construct a variance function which describes the amount of variance in any given wind direction. This can be found by using a modification of the orographic spectrum function ideas employed by the Unified Model gravity wave scheme (see e.g.Gregory et al. 1998; Webster et al. 2003).

As derived in Dean et al. (2005) the unresolved surface variance σ, for a wind direction χ can be expressed as

$$\sigma(\chi) = C[(4\cos^2\chi - 1)\sigma_{xx} + (4\sin^2\chi - 1)\sigma_{yy} + 8\sigma_{xy}\sin\chi\cos\chi] \quad (1)$$

where σ_{xx} and σ_{yy} are the squared sub-grid zonal and meridional orographic elevation gradients, respectively, and σ_{xy} is the covariance between zonal and meridional elevation gradients. C is a constant which includes a representation of the the unresolved horizontal scales in the model, and is hence model-dependent.

The new parameterisation follows Palmer et al. (1986) in defining a surface layer of air. The peak height of the unresolved topography h_m, is assumed to be related to the directional surface variance by

$$h_m = 2\sigma^{1/2}(\chi) \quad (2)$$

The nearest model level to this height is taken to be the top of the surface layer. However, the effective height of the unresolved orography may be reduced by flow blocking. The fundamental parameter that controls flow blocking is the Froude number Fr, defined here as

$$Fr = \frac{U}{Nh_m} \quad (3)$$

where U is the horizontal wind speed and N the static stability. Since the Froude number can be interpreted as a ratio of the kinetic to potential energy of an air parcel (Leung and Ghan 1995), the maximum height rise of a parcel occurs when the Froude number is equal, or very close, to unity. Thus the initial maximum peak vertical displacement amplitude of the unresolved gravity wave $A(0)$, is chosen to be

$$A(0) = \min\left[h_m, \frac{U}{N}\right] \quad (4)$$

The bottom of the surface layer is defined to be the model level closest to the height of any blocked layer h_b, where

$$h_b = h_m - \frac{U}{N} \quad (5)$$

2.2 Vertical propagation and wave saturation

In the absence of damping, gravity waves will grow in amplitude due to the decreasing density of the atmosphere with height. Using WKBJ theory McFarlane (1987) showed that the evolution of the vertical displacement amplitude of a linear wave is governed by

$$A(z) = A(0)\left(\frac{\overline{\rho}(0)N(0)U(0)}{\overline{\rho}(z)N(z)U(z)}\right)^{\frac{1}{2}} \quad (6)$$

where $\overline{\rho}(z)$ is the background density. In the parameterisation the amplitude of the wave must be calculated iteratively upwards through the model levels. As such a modification of Eq. 6 is used:

$$A_k = A_{k-1}\left(\frac{\overline{\rho}_{k-1}N_{k-1}U_{k-1}}{\overline{\rho}_k N_k U_k}\right)^{\frac{1}{2}} \quad (7)$$

where k is an index for model levels that increases with increasing altitude. However, amplitude growth cannot occur in an unrestricted way. At some height the wave could reach amplitudes for which the wave field becomes unstable (Lindzen 1981). At this "saturation amplitude" the turbulence generated inhibits any further amplitude growth. For convective instability this means that the lapse rate due to the sum of the mean state and wave perturbations has become equal to the adiabatic lapse rate. The general Richardson number is used to describe where and when turbulence will occur. The local wave-modified Richardson number Ri_m, can be written in terms of the background Ri_b, U, N and peak wave vertical displacement amplitude A, (Palmer et al. 1986) as

$$Ri_m = \frac{Ri_b(1 - \frac{NA}{U})}{(1 + \sqrt{Ri_b}\frac{NA}{U})^2} \quad (8)$$

If wave breaking is said to occur for $Ri_m < 0$, the criterion for convective instability, then Eq. 8 can be used to find the saturation amplitude

$$A_s = \frac{U}{N} \quad (9)$$

This is the saturation condition employed in this scheme and follows McFarlane (1987) and Bacmeister et al. (1994). In practice this saturation constraint is expressed as

$$A_k = \min\left[A_k, \frac{U_k}{N_k}\right] \tag{10}$$

Additionally if the wind component in the direction χ becomes zero at any level then the amplitude is set to zero at all levels above this, as this corresponds to complete mountain wave absorption at a critical level.

2.3 Wave displacement

The actual vertical displacement produced by a wave at various heights above a mountain depends on both wave amplitude and phase. As a result air displacement can be both upward and downward, with associated cooling or heating, respectively. For an orographic cloud parameterisation acting in the troposphere it is useful to know where such cooling and warming will occur. The approach in this parameterisation is to represent the average displacement across a grid-box as being generated by an ensemble of separated, bell shaped ridges.

Queney (1948) derived analytical two-dimensional mountain wave solutions for a one-layer model of constant stability N and constant flow U across a bell shaped mountain of peak height h_m and half-width a. We generalise that solution by using WKBJ methods in which U and N are now allowed to vary slowly in the vertical (compared to wave phase). This leads to a 2D vertical displacement of the form

$$\eta(x,z) = A(0)a\left(\frac{\overline{\rho}(0)U(0)N(0)}{\overline{\rho}(z)U(z)N(z)}\right)^{1/2} \times \left(\frac{a\cos\phi - x\sin\phi}{a^2+x^2}\right) \tag{11}$$

where x is the horizontal distance downstream of the mountain peak and the lower boundary condition is $A(0)$ as given by Eq. 4. The wave phase $\phi(z)$, is derived as the integral with respect to height of the Scorer parameter $l(z)$, where

$$l^2(z) = \frac{N^2(z)}{U^2(z)} + \frac{1}{U(z)}\frac{\mathrm{d}^2U(z)}{\mathrm{d}z^2} \tag{12}$$

The assumption of slowly varying N and U allows the second derivative term to be ignored such that

$$\phi = \int_0^z l\,\mathrm{d}z = \int_0^z \frac{N(z)}{U(z)}\,\mathrm{d}z \tag{13}$$

This WKBJ generalization of Queney's single-layer Fourier integral solution requires that it can be adequately approximated using the method of stationary phase. Formally, the stationary phase approximation fails for 2D hydrostatic irrotational mountain wave solutions, since each individual hydrostatic wave mode of differing horizontal wavelength propagates purely vertically above the mountain, producing phase overlap and caustic singularities (see, e.g. Fig. 2a and accompanying discussion in Broutman 2004). However, if we ignore horizontal geometric spreading, and assume that wave energy radiated from the mountain is concentrated sharply at a dominant horizontal wavelength determined by the mountain half-width a, then Eq. 11 will provide an adequate approximation to the true mountain wave field. Indeed, such approximations are implicit in all existing vertical column parameterisations of orographic gravity wave drag.

In order to implement this solution as a parameterisation, we need to consider the average effect within a model grid box. Our approach here is to compute the average vertical displacement of a streamline at a given height within the grid box by averaging Eq. 11 along the horizontal direction, i.e.

$$\eta_{\mathrm{mean}}(z) = \frac{1}{2L}\int_{-L}^{L} \eta(x,z)\,\mathrm{d}x \tag{14}$$

where L is the averaging length, which can be interpreted as half the typical spacing between adjacent sub-grid scale ridges within a grid box. This integration yields a final solution of the form

$$\eta_{\mathrm{mean}}(z) = \frac{A(0)a}{L}\left(\frac{\overline{\rho}(0)U(0)N(0)}{\overline{\rho}(z)U(z)N(z)}\right)^{1/2} \times \arctan\left(\frac{L}{a}\right)\cos\phi \tag{15}$$

The inclusion of the bell shaped ridge leads to the introduction of two arbitrary parameters that describe the 'average' ridge and must be specified. Here the ridge spacing and half width are given the initial values of $2L = 60$ km and $a = 10$ km, but are ultimately tunable. Such ridge parameters are common in gravity wave schemes which explicitly calculate amplitude (cf. α and L parameters in Bacmeister et al. 1994).

But does Eq. 15 make sense in terms of the effect on cloud formation? Queney (1948) presents the solution streamlines for flow over a bell shaped ridge with constant N and U in the vertical. When the streamlines for this result are considered some undergo only upward displacement and would potentially show only cloud formation. Others show only downward displacement and thus potential cloud evaporation. Some show a mix of both. In all of these cases the average

displacement will give the right effect of overall potential cloud formation or destruction only if there is no hysteresis in the evaporation of cloud. In certain atmospheric conditions this is not always the case.

Because the upper troposphere is often deficient in ice nuclei the air can regularly be supersaturated. If an air parcel is supersaturated with respect to ice, but undersaturated with respect to water, and during a streamline ascent it reaches water saturation, then ice will rapidly form and survive downstream of the wave. Additionally, if during ascent, an air parcel cools to about –40°C, then homogeneous nucleation may be initiated and ice can rapidly form which will survive downstream of the wave. These two processes are believed to be important in the creation of very large orographic cirrus clouds and so are incorporated in the parameterisation. In both cases it is the maximum vertical displacement of the streamline that is critically important. Thus, if either condition is satisfied for the maximum displacement, then this is used to calculate the temperature perturbation. Otherwise the average displacement is used. It should be noted that the maximum displacement may also be important for orographic clouds which precipitate, but this is not considered in this paper.

The maximum wave-induced displacement at a given altitude z is where

$$\frac{\partial \eta(x,z)}{\partial z} = 0 \tag{16}$$

which after differentiating Eq. 11 can be seen to be satisfied by,

$$x = a\left(\frac{\cos\phi \pm 1}{\sin\phi}\right) \tag{17}$$

It can then be verified that the choice of the negative sign gives the maximum displacement and the positive sign the minimum. Substituting this solution into Eq. 11 gives the maximum wave-induced displacement as

$$\eta_{max}(z) = A(0)\left(\frac{\overline{\rho}(0)U(0)N(0)}{\overline{\rho}(z)U(z)N(z)}\right)^{\frac{1}{2}} \times \left(\frac{\sin^2\phi}{\sin^2\phi + [\cos\phi - 1]^2}\right) \tag{18}$$

To calculate the displacement it is necessary to integrate the phase iteratively up to the current level. Using the trapezoidal rule Eq. 13 can be approximated as

$$\phi_k = \phi_{k-1} + \frac{\Delta z}{2}\left(\frac{N_{k-1}}{U_{k-1}} + \frac{N_k}{U_k}\right) \tag{19}$$

where Δz is the difference in height between the layer centres. The mean and maximum displacement for a level can then be calculated as

$$\eta_k^{\text{mean}} = A_k \frac{\cos\phi_k \arctan\left(\frac{L}{a}\right)}{L} \tag{20}$$

$$\eta_k^{\text{max}} = A_k \frac{\sin^2\phi_k}{\sin^2\phi_k + (\cos\phi_k - 1)^2} \tag{21}$$

To first order, the temperature perturbations caused at each level by the displacements can be calculated from the local potential temperature gradient under the assumption of adiabatic vertical parcel displacement. See Eckermann et al. (1998) for validation of this assumption based on adiabatic parcel advection modelling under the influence of gravity waves.

3 Implementation in the Unified Model

The parameterisation has been implemented in the HadAM3 version of the Unified Model, which has a 2.5° by 3.75° horizontal resolution and 19 levels in the vertical. This configuration is an atmosphere-only model and has prescribed sea surface temperatures. A full description of the model can be found in Pope et al. (2000). The simulation shown here included the so-called 3B mixed phase precipitation scheme and 2B cloud scheme with a prognostic ice variable as described by Wilson and Ballard (1999).

To describe the hydrological cycle the model advects three prognostic variables: the liquid + vapour water content, the ice water content and the 'liquid' temperature (the temperature the air would have if the liquid was evaporated). The ice cloud fraction is diagnosed at each time step for each layer as a function of the ice water content (stored as a mixing ratio), taking into account subgrid variability through a triangular probability distribution function. The liquid cloud fraction, cloud liquid water, and hence temperature, are diagnosed in a similar way from a triangular distribution of total water content minus saturation water content. The width of the triangular distribution is parameterized in terms of the larger scale cloud variability (see, Cusack et al. 1999).

The original mixed phase precipitation scheme in the Unified Model simply diagnosed the amount of ice and liquid water at each timestep by using a temperature function. In the 3B scheme used here the inclusion of a prognostic ice variable allows not only for the calculation of an ice cloud fraction, but also for the introduction of ice microphysics which describe how

ice is transferred from one state to another. The amount of ice in a grid box is predicted by growing and decaying it from and to liquid, vapour, and rain. The transfer processes are outlined in Wilson and Ballard (1999). In theory this should allow for the creation and survival, at least microphysically, of orographic cirrus clouds. Convective cloud and precipitation are calculated in a separate routine and are not considered in this paper.

The orographic parameters used by the parameterisation are the standard set for this version of the Unified Model and are derived from the US Navy 10' topographical dataset. Detail on the calculation of the subgrid orographic gradients can be found in Dean et al. (2005).

The temperature perturbations calculated by the parameterisation are used in both the cloud scheme and mixed phase precipitation scheme. While there may be a justification in adding a temperature perturbation to other selected physics parameterisations each would have to be analysed on an individual basis. In restricting its application we have made interpretation of the resulting changes in the simulation simpler. From a dynamical perspective, while it is tempting to allow the temperature perturbation to be visible to the large-scale dynamics, we have not done so because our parameterisation only captures vertical perturbations and not horizontal perturbations within the grid box and downstream. Thus we believe that the dynamic filter applied at each time step for stability reasons would smooth the temperature perturbations out over an inappropriately large scale and lead to unrealistic large-scale responses. At this stage of maturity we think the larger scale responses should come through the physics.

While the perturbation could be applied to only the ice physics, it is useful to apply it to the the entire mixed phase precipitation subroutine. Doing so is expected to have the secondary benefit of increasing the amount of rainfall over high orography, since the gravity wave scheme will predict considerable uplift adjacent to the mountains. This is in contrast to the artificial thresholds currently used in many precipitation schemes (mostly to account for changes in condensation nuclei over land), but may not be as effective as the sub-grid orographic precipitation scheme of Leung and Ghan (1995) and (1998).

The parameterisation has been tested with idealised profiles to show that it can accurately reproduce analytical results. A more stringent test of the ability of the linear hydrostatic gravity wave scheme to predict reasonable temperature perturbations is now made using a mesoscale model.

4 Realistic profile over the Andes

Tan nad Eckermann (2000) have used a two dimensional, nonlinear, high resolution, compressible model to study mountain waves over the Andes. The simulations used realistic upstream profiles of wind and temperature to calculate the temperature perturbation due to waves in the middle atmosphere. These were then compared with the temperature profiles measured by an infrared satellite limb scanner at the same time. The model uses a single transect taken perpendicular to the main axis of the Andes. Since the Andes were identified as an area of orographic cirrus generation in Dean et al. (2005) such waves are also likely to lead to cirrus generation in the troposphere. In fact, photos taken by shuttle astronauts during this event showed a long band of cirrus-like cloud running along the Andean spine (Eckermann and Preusse 1999). Here we now compare the temperature perturbations predicted by the parameterisation with those predicted by the mesoscale model for the same event.

It is first necessary to choose an appropriate gridbox to use for the comparison. The horizontal line in Fig. 1 represents the zonal transect that is closest to that of the mesoscale model, transposed onto the UM domain. The sub-grid topography parameters needed for the parameterization are taken from the arrowed gridbox.

Figure 2 shows the upstream profiles of wind speed (perpendicular to the mountains), temperature and stability using the data of Tan and Eckermann from NASA's Data Assimilation Office. Also shown are the profiles interpolated onto the resolution of the Unified Model (19 levels). The profiles are resolved reasonably well, although deviations are somewhat damped.

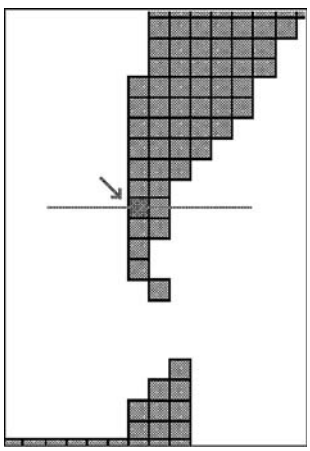

Fig. 1 Transect across the Andes similar to that used by Tan and Eckermann transposed onto the Unified Model grid. The *arrow* indicates the gridbox used for the comparison

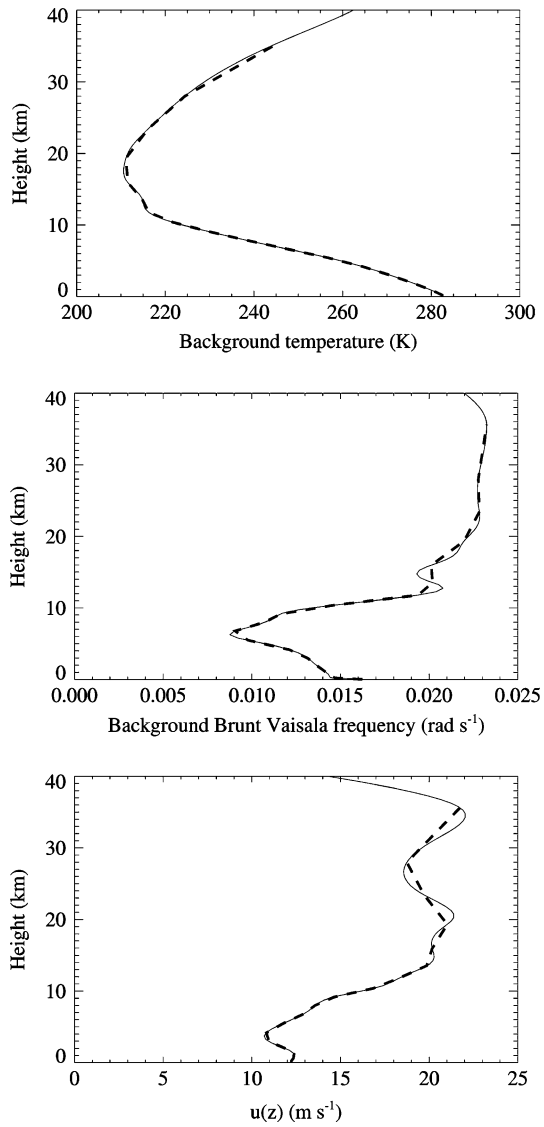

Fig. 2 The input fields used as the upwind boundary condition for the Tan and Eckermann model (*solid line*) and the fields interpolated onto the Unified Model's 19 levels (*dashed line*)

Given the atmospheric profiles from Fig. 2, and the Unified Model sub-grid orographic parameters for the gridbox identified in Fig. 1, the temperature perturbation predicted by the parameterization is the dashed line in Fig. 3. The solid line is the result predicted by the mesoscale model averaged across the transect at full vertical resolution in (a) and at the resolution of the Unified Model in (b).

The agreement in vertical wavelength, amplitude and phase is excellent, especially below 20 km. The disagreement above 20 km is not a major concern as there are only three model levels above this point. This results in very poor resolution of the wave oscillation vertically (as shown by panel b). The most important result is the good prediction of significant cooling of a similar magnitude in the upper troposphere by both the mesoscale model and the parameterisation.

5 Observations of an orographic cloud over New Zealand

Here we use satellite data to investigate possible orographic cloud effects over New Zealand, as an observational gauge prior to testing our parameterization in the same geographical region.

New Zealand is not unique in generating large orographic cirrus clouds, but its narrow land mass and high mountains make it an ideal testbed for studying relatively simplified mountain flows and the resulting clouds that form. In particular the mountain ranges of the South Island of New Zealand present a high barrier to the mid-latitude westerly flow. Many of the mountain ranges are over 1,000 m high and Mt Cook, the highest peak, stands at 3,754 m. The combination of the steep land mass and surrounding ocean also results in relatively little convective activity to confuse the interpretation of orographic wave clouds.

Anticyclones and depressions pass over New Zealand regularly from the west. Strong north-westerly winds occur over the South Island when an anticyclone is located to the north-east of New Zealand and a depression to the south-west. There is also often an associated cold front. These north-west winds can persist for a number of days and result in airflows which are perpendicular to the main long ridge axis of the mountain ranges. In such a situation a solid sheet of cloud often forms downwind of the mountains for distances which can range from tens to hundreds of kilometres.

The synoptic situation for a case in which such a cloud was observed is shown in Fig. 4. The mean sea level pressure chart for 1200 GMT on the 1 July 1999 reveals a strong northwest flow over the South Island with a deep depression to the south west and a trough lying in the Tasman sea directly to the west of New Zealand. Figure 5 is imagery from the NOAA-14 polar orbiting satellite at 0353 GMT on the 1 July 1999. This daytime image is a composite of three of the advanced very high resolution radiometer (AVHRR) Bands. Band 1 (visible), 2 (near infrared) and 4 (micron infrared) are displayed as blue, green and red, respectively, after calibration. Band 4 is calibrated to brightness temperature with black being warm and white cold. The overall effect is for vegetation to turn up green, and dense cold (high) clouds as white. Cirrus cloud, which is semi transparent at visible wavelengths, appears red while warmer low clouds have a blue tint.

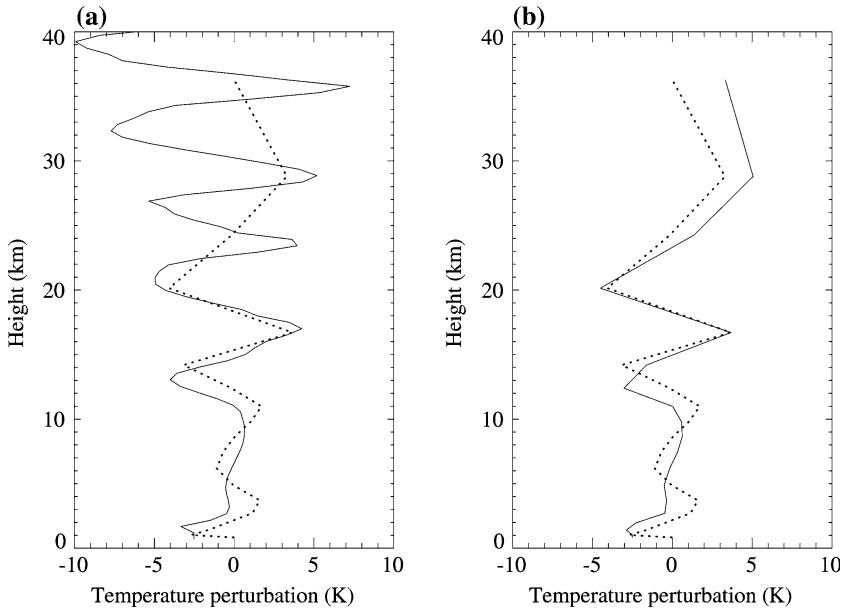

Fig. 3 Comparison between the mean temperature perturbation predicted by the high resolution model (*solid line*) along the transect, and the parameterisation (*dashed line*). In **b** the mesoscale model result is interpolated onto the UM grid

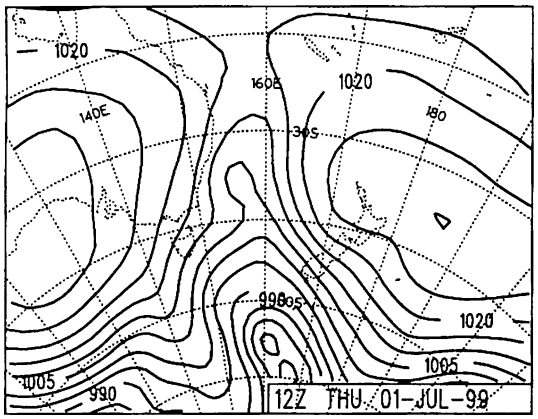

Fig. 4 Mean sea level pressure chart for 1200 GMT on the 1 July 1999

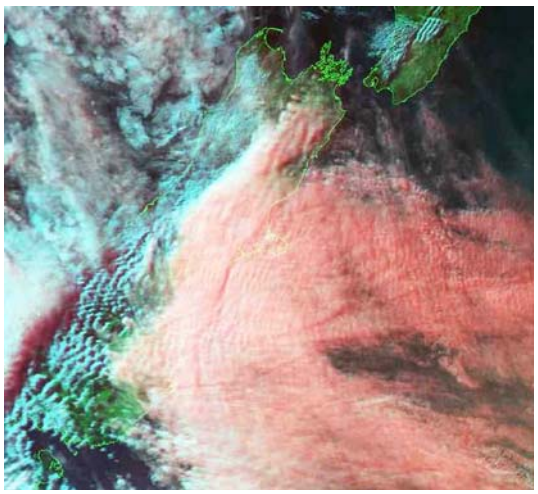

Fig. 5 NOAA-14 AVHRR composite image of channels 1, 2 and 4 over the South Island of New Zealand at 0353 GMT on the 1 July 1999. From http:// www.satellite.landcareresearch.co.nz/noaa/

Depending on ground temperatures snow may also have a bluish tint. In this image a high level orographic cloud can be seen forming over the mountains and being advected downstream with a decreasing optical thickness.

Figure 6 is an infrared image (10.3–11.3 μm) from the geostationary meteorological satellite (GMS-5). Here it can be seen that the cloud in Fig. 5 is of sufficient size to be globally significant, especially considering the foreshortening that occurs at the limb of such images. Cloud associated with a cold front can be seen clearly over the Tasman Sea.

Such clouds are relatively frequent (Ridley 1991) and this particular case is chosen principally because of the availability of a wide set of observations. Figure 7 shows observed radiances and retrieved measurements from an overpass of the along track scanning radiometer 2 (ATSR-2) instrument on board ERS-2 at 2227 GMT on the 30 June 1999. ATSR-2 is a dual angle imaging radiometer measuring at 1 km resolution with four visible channels centred at 0.55, 0.67, 0.85 and 1.6 μm and three infrared channels at 3.7, 11 and 12 μm. In panel (a) the 11 μm channel is presented as a brightness temperature. In panel (b) the 0.67 μm channel is presented as an albedo. At this time the orographic cloud is less developed than in Fig. 5. Where the cloud is optically thick (green in panel b) the brightness temperature in panel (a) is a reasonable estimate of the cloud top temperature. A radiosonde

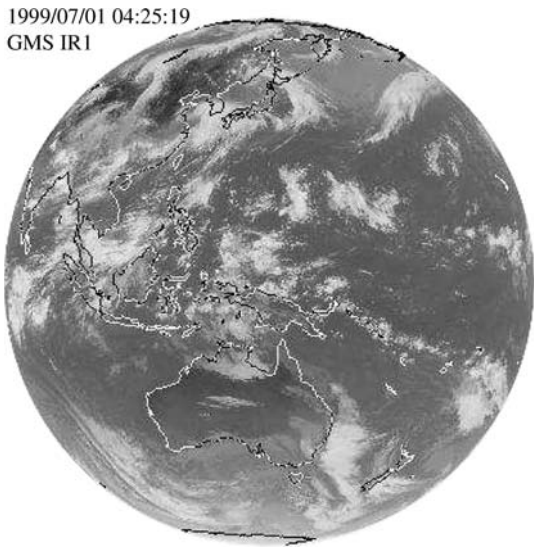

Fig. 6 Infrared image from GMS-5 at 0425 GMT 1 July 1999 when the trailing orographic cloud off New Zealand was at its largest extent

observation near this time placed the tropopause at 200 mb at a temperature of 205 K, implying that the cloud top is at the tropopause. This is confirmed in panels (c) and (d), which present the cloud top pressure and cloud water path from a full optimal estimation retrieval as described in Watts (1995).

For comparison, data from the International Satellite Cloud Climatology Project (ISCCP) D1 dataset at 0000 GMT over the immediate New Zealand region is included in Fig. 8. ISCCP D1 data are generally a merging of cloud products retrieved from various satellites, though for this time and place the data are an hourly mean of GMS-5 observations averaged to a 2.5° resolution. The cloud fraction, (a), is high to the south west of New Zealand and much lower to the north east. In (b) it can be seen that only to the immediate east of New Zealand is the total cloud dominated by high cloud (defined as a mean cloud top pressure lower than 440 mb). A smaller proportion of cloud to the west is also classified as high cloud. In (c) the cloud top

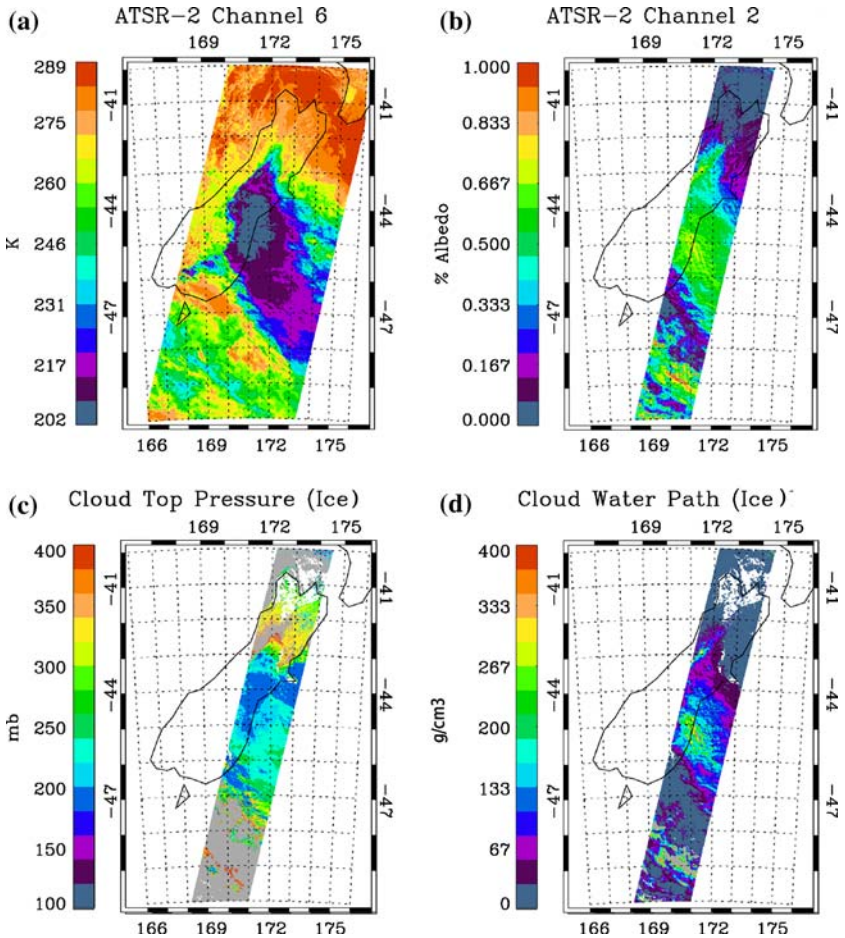

Fig. 7 ATSR-2 observations over the South Island of New Zealand at 2227 GMT on the 30 June 1999. **a** The 11 μm brightness temperature, **b** the 0.67 μm albedo, **c** the retrieved cloud top pressure (mb) and **d** the cloud water path (g cm^{-3})

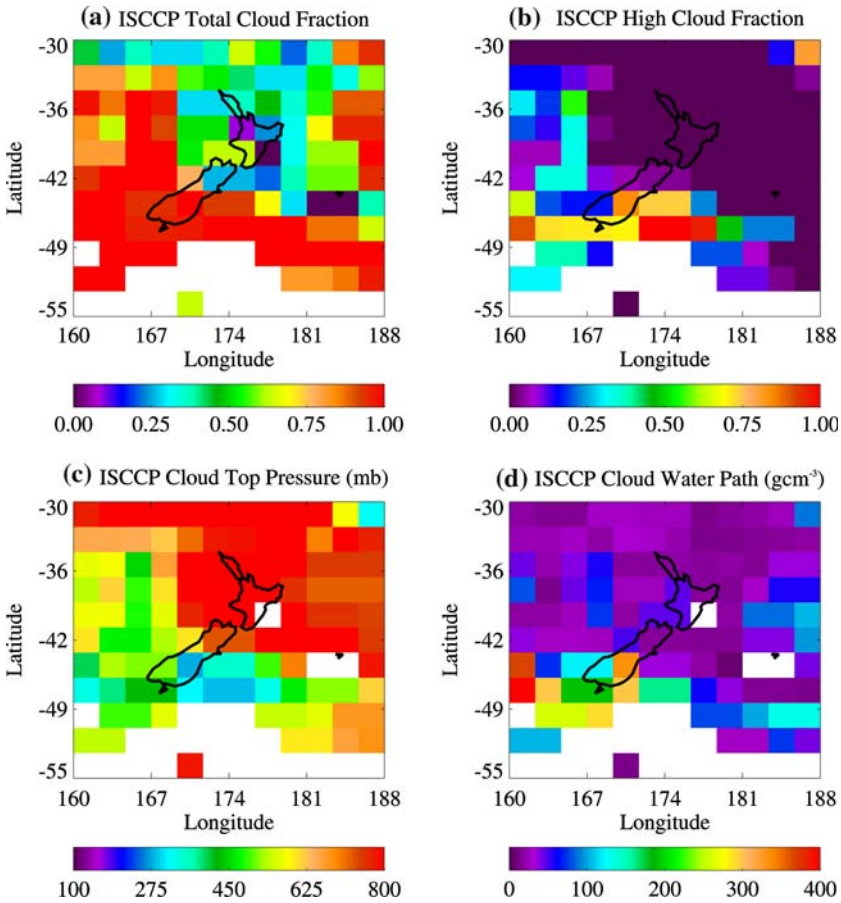

Fig. 8 ISCCP D1 hourly mean parameters over the New Zealand region at 0000 GMT on the 1 July 1999. These include **a** total cloud fraction, **b** high cloud fraction **c** cloud top pressure (mb) and **d** cloud water path (g cm^{-3})

pressure can be seen to be very low (around 250 mb) only in the area of the distinct orographic cloud. While this is not as low as in the ATSR-2 retrieval (minimum of 200 mb) the averaging process in ISCCP will act to increase the cloud top pressure from the minimum if the 2.5° grid box is in any way inhomogeneous. The cloud water path (d) is similar to that for ATSR-2 though with a high bias.

ISCCP also provides a cloud fraction for cirrus, which is defined as those pixels in a grid box which have cloud top pressures in the range 10–440 mb and optical depths of 0.02–3.55 (Fig. 9). From this breakdown it can be seen that, while the cloud is optically thick directly over the mountains, it is the downstream advection that leads to the formation of orographic cirrus. This result emphasises that orographic gravity waves are a plausible mechanism for the generation of large scale cirrus clouds downwind of major mountain ranges as identified by Dean et al. (2005). The apparently slow evaporation of the cirrus cloud generated suggests that the air upwind of the mountains in the upper troposphere was below, but very close to, the saturation point with respect to ice.

In conclusion, a body of observational evidence from satellites has been drawn together to understand a case study of a large scale orographic cloud over New Zealand. The cloud top is located at or near the tropopause and has significant water paths over the mountains. The ice created is advected for

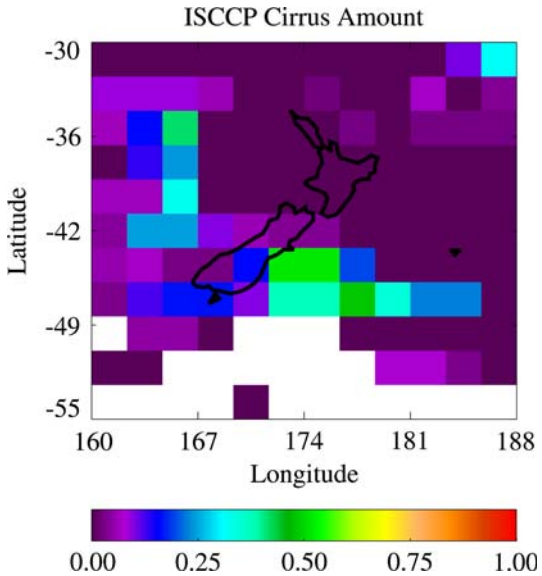

Fig. 9 ISCCP D1 cirrus fraction over the New Zealand region at 0000 GMT on the 1 July 1999

considerable distances downwind to create large scale cirrus clouds. In the next section we address the ability of the Unified Model to produce such clouds with and without the parameterisation described earlier.

6 Nudging experiment

Attempts to evaluate model cloud behaviour often rely on statistical comparisons between time averaged model fields and observations, or evaluation against case studies in high resolution models. This can make interpretation of results difficult when it is not clear if discrepancies arise because of problems in the cloud parameterisation, other model physics, or the underlying dynamical regime. In this paper we utilise a methodology which mimics ''real'' events by ''nudging'' GCM winds, temperatures and humidities towards those of the ERA-40 analysis (ECMWF 1995). This analysis acts as a proxy for numerous underlying observations, with issues of heterogeneity, quality control and covariance estimation already taken care of. A similar methodology was developed by Jeuken et al. (1996) for the ECHAM4 model and used by Feichter and Lohmann (1999) to validate two different cloud physics parameterisations.

6.1 Method

At each timestep four of the models prognostic fields (winds, temperature and specific humidity) are adjusted by 20% of the difference between their current state and the corresponding values interpolated both spatially and temporarily from the ERA-40 dataset. Analysis has shown that convergence of the nudged fields between the model and ERA-40 occurs after a couple of days with RMS errors of less than 1 m s^{-1} in wind and 1 K in temperature (zonal and meridional averages).

6.2 Nudged control

Here we use the technique within the Unified Model to recreate the dynamic conditions present at the time of the orographic cloud event described in Sect. 5. The nudging experiment is begun on the 1 June 1999 to ensure full convergence of the fields by the time of the orographic cloud event on the 1 July. In Fig. 10 are the model profiles of zonal wind (u), meridional wind (v), temperature (T) and specific humidity (q) for the southernmost of the three New Zealand gridboxes for the timestep corresponding to 0000 GMT on the 1 July 1999 (dashed lines). This is the time of the ISCCP observations in Fig. 8 and within 90 min of the ATSR-2 overpass. For comparison the spatially interpolated profiles from ERA-40 for the same time are presented as solid lines. For each of the fields the agreement is remarkably good, though not perfect.

The structure of the wind fields is captured well and it is clearly apparent that a strong north-westerly airflow lies over New Zealand at all heights in the troposphere. Deviations are generally less than 2 m s^{-1} with a maximum of 4 m s^{-1} in the troposphere. The model temperature is within 1.5 K of ERA-40 in the troposphere. A radiosonde profile launched from Invercargill, New Zealand (–46.70 S, 168.55 E) at the

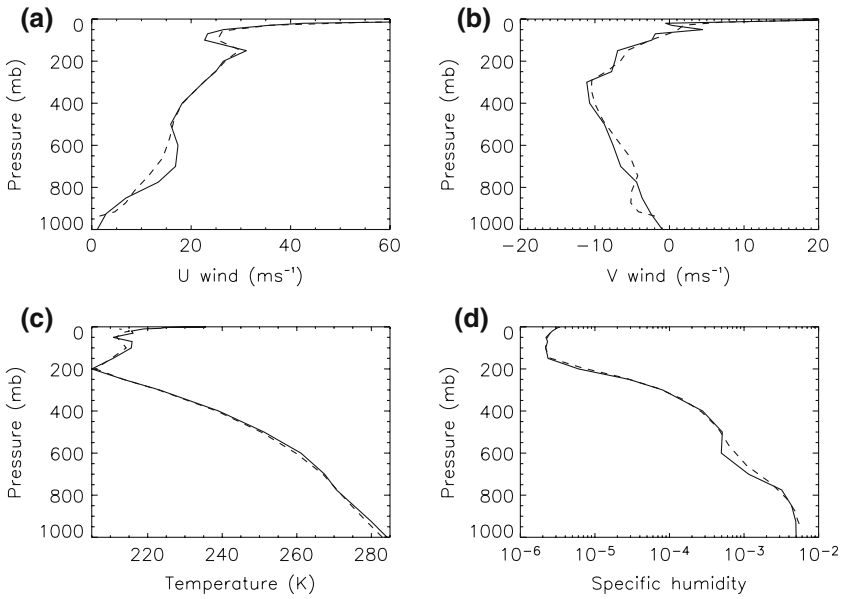

Fig. 10 The Unified Model profiles (*dashed lines*) from the nudged control run of **a** the zonal wind u, **b** the meridional wind v, **c** temperature and **d** specific humidity over the southernmost New Zealand gridbox at 0000 GMT on the 1 July 1999. Also shown are the ERA-40 profiles for the same time interpolated onto the Unified Model domain (*solid lines*)

same time shows deviations of similar magnitude from both ERA-40 and the nudged model. The specific humidity is plotted on a logarithmic scale and shows some deviation in the lower troposphere, though it appears that the model profile is simply smoother.

Figure 11 shows the model fields for total cloud, high cloud, cloud top pressure and cloud water path at 0000 GMT on the 1st July 1999. This is the same time as the ISCCP observations in Fig. 8. The total cloud amount is not nudged but is instead diagnosed from the amount of simulated cloud in each model level under the assumption of a maximum random overlap. Each panel will be discussed in turn for clarity:

(a) Compared to the ISCCP observations the model has less total cloud cover. This has been observed as a consistent response in all of our simulations where the model is nudged with ERA-40 specific humidities.

(b) The dominant contribution to the simulated total cloud cover is the significant amount of high cloud, which is considerably greater than that seen in the observations.

(c) The cloud top pressure shown is not analogous to the ISCCP cloud top pressure but should instead be interpreted as simply the pressure of the top model level which contains cloud. This indicates that in much of this geographic region the upper-tropospheric levels of the model contain at least some cloud.

(d) The water path shown does not include the contribution from the convective cloud in the Unified Model, which is often very large. This makes it quantitatively inaccurate but allows a better qualitative comparison with the ISCCP observations. Most importantly there is some evidence of an increase over the southernmost grid box. Analysis has shown that this is primarily due to an increase in the low level cloud over the southernmost New Zealand land point compared to gridboxes upwind and downwind. This increase in cloud is most likely a consequence of the cooling that occurs as the air is lifted over the orography.

The model appears to have been forced into a dynamical situation where orographic clouds such as

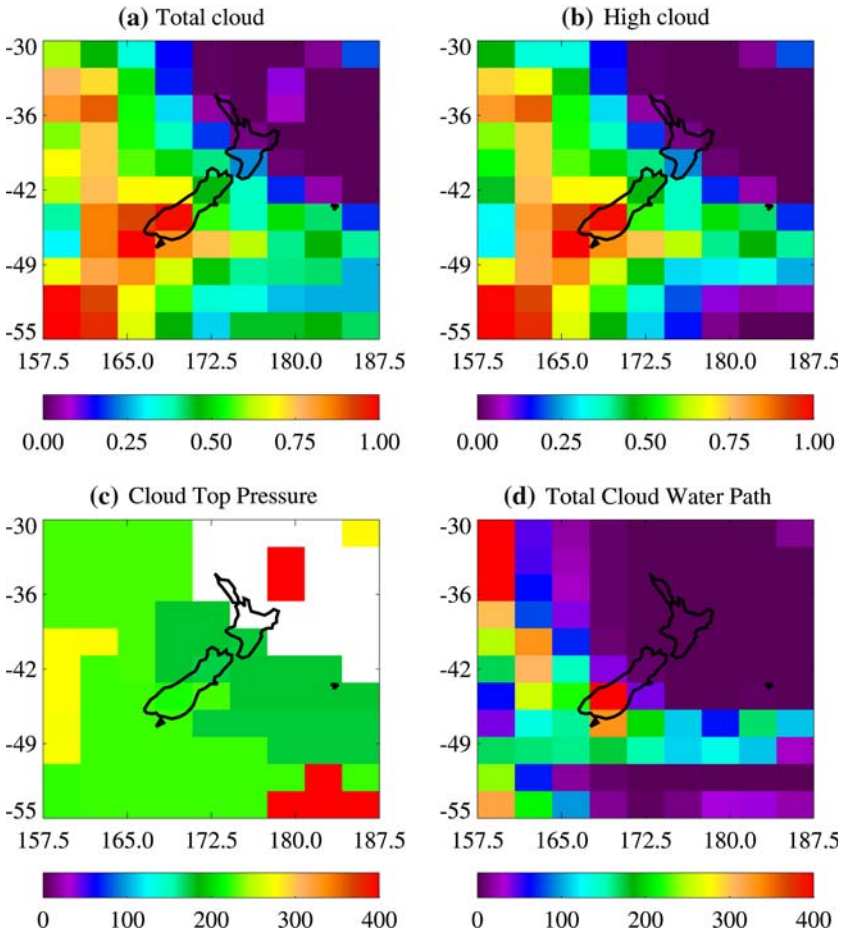

Fig. 11 Nudged control run fields for **a** total cloud fraction, **b** high cloud fraction, **c** cloud top pressure (mb) and **d** cloud water path (g cm^{-3}) at 0000 GMT on the 1 July 1999

those identified in Fig. 5 should form. However, the model has produced significant high cloud to the west of New Zealand, which is considerably greater than that in the observations. This makes interpretation of the cloud cover over New Zealand more difficult. The north-west flow will be bringing warm moist air south from the sub-tropics. Whether upper level clouds form in this airflow depends critically on the temperature, rate of moisture transport and the presence of any ice supersaturation due to a lack of ice nuclei. Investigations have shown that in the regions of excess high cloud both the model and ERA-40 are sub-saturated with respect to ice and water, though ice saturation is about 95% in the model. As discussed in Sect. 5, the geographical extent of the orographic cloud deck in the satellite observations suggests that the upper troposphere upwind of New Zealand must have been close to ice saturation, thus supporting the assumption that ERA-40 is reasonable. It is possible that the ice microphysics of the model are not able to accurately resolve this pre-frontal situation.

Regardless, there is no significant increase in high cloud over the land or downwind, as seen in the observations. This is not unexpected, as the model should not be able to reasonably resolve the gravity wave from an obstacle that is only one gridbox wide. Thus there is still a deficiency due to the lack of representation of orographic gravity waves.

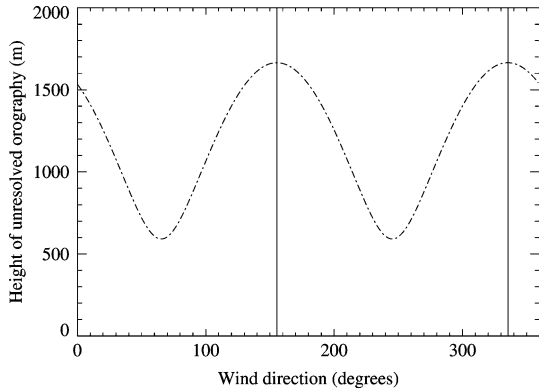

Fig. 12 The peak height h_m, of the unresolved orography for the southernmost New Zealand gridbox and all wind directions (*dashed line*). The wind directions with the peak response are indicated (*solid lines*)

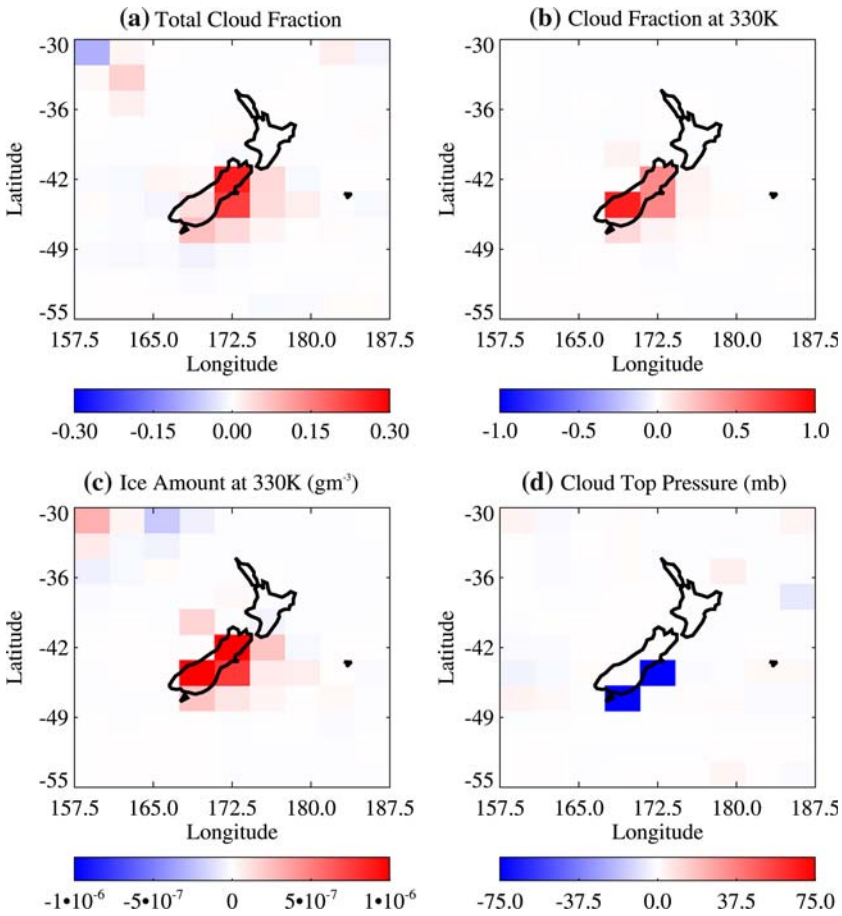

Fig. 13 Difference in certain Unified Model fields at 0000 GMT on the 1 July 1999 between the control simulation and the simulation with the parameterisation included for **a** total cloud fraction, **b** cloud fraction interpolated onto the 330 K potential temperature surface (250 mb), **c** ice amount interpolated onto the 330 K potential temperature surface (250 mb), **d** cloud top pressure

6.3 Nudged parameterisation

An additional simulation was performed with identical conditions, apart from the inclusion of the parameterisation described in Sect. 2.

Figure 12 is the peak height of the unresolved orography for the southernmost New Zealand gridbox showing all wind directions, as predicted by Eq. 2. There is a peak of 1,600 m in the height of the unresolved orography at wind directions of 155° and 335°. This is in good agreement with the qualitative idea that orographic cirrus clouds are produced in this region when there are strong northwest winds and should ensure that parameterization responds strongly in the northwest flow reproduced in the nudging experiment.

Figure 13 is the difference in, (a) total cloud fraction between the control and parameterisation run at 0000 GMT on the 1 July, (b) difference in cloud amount on the 330 K potential temperature surface, (c) difference in ice amount, also at 330 K and, (d) the difference in cloud top pressure. The total cloud fraction has increased significantly over one New Zealand gridbox, as well as to the east of New Zealand. This was found to be due to the successful advection of extra ice into the adjacent gridboxes in the upper troposphere and the subsequent increase in cloud, as illustrated by (b) and (c). Because transport of ice should occur along isentropic surfaces, rather than the hybrid model levels, the fields are shown for the 330 K potential temperature surface. Other surfaces in the upper troposphere show a very similar pattern. Over the southernmost land gridbox the total cloud fraction was already almost 1 so increases were smaller despite the increase in ice. The change in cloud top pressure simply illustrates that in three of the gridboxes clouds and ice were introduced into a higher level of the model to the east of New Zealand.

In Fig. 14 are the vertical profiles of a number of fields for the southernmost New Zealand gridbox at 0000 GMT on the 1 July 1999. In (a) the amplitude at each model level is plotted against the pressure at that level. The amplitude growth or decay is essentially constrained by changes in the windspeed and stability with height. The changing phase means that strong

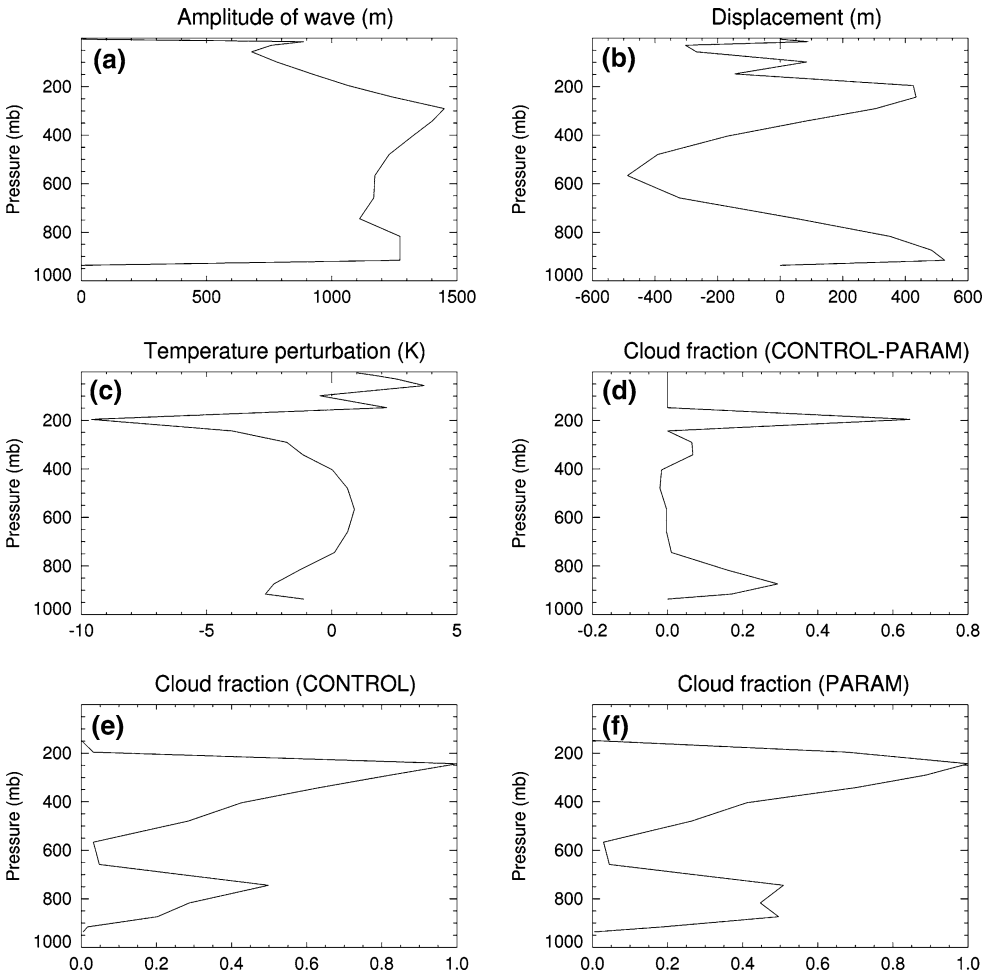

Fig. 14 Profiles of model fields over the southernmost New Zealand gridbox:**a** amplitude of the sub-grid hydrostatic gravity wave predicted by the parameterisation, **b** the displacement induced at each level by this wave, **c** the equivalent temperature perturbation, **d** the difference in cloud fraction with and without the parameterisation, **e** the unperturbed cloud amount profile and **f** the perturbed cloud profile

upward displacement (b) of the air occurs close to the mountains, a downward displacement in the middle troposphere and an upward displacement in the upper troposphere. These displacements are translated into temperature perturbations (c) for which the dominant effect is a strong cooling throughout the upper troposphere and particularly near the tropopause at 200 mb. When these temperature perturbations are included in the cloud scheme they lead to an increase in cloud at low levels and near the tropopause (d). For completeness the cloud amount in the control run for each layer and the perturbed cloud profile are also shown (e and f). It is apparent that the only reason a significant increase in cloud is not seen over this gridbox is because of the pre-existing ice cloud in the upper troposphere. It is possible that, were the upper level ice cloud not so significant already, the scheme would cause a greater change in cloud, at least for the land gridboxes. This has been investigated, in a somewhat qualitative way, by extracting the model profiles from the control simulation for the southernmost New Zealand gridbox at the timestep of interest. The profiles were then adjusted by evaporating the ice present, adding the subsequent vapour to the specific humidity and updating the temperature due to the release of latent heat. The Unified Model cloud parameterization and some of the microphysics are then used, external to the model, to calculate the amount of cloud that would be diagnosed. Figure 15a shows that in the absence of pre-existing ice the cloud scheme would diagnose only a small amount of ice cloud, created mostly by the freezing of liquid water . However, after inclusion of the temperature perturbation, as calculated by the new gravity wave parameterisation, the cloud scheme diagnoses a significant ice cloud layer in the upper model levels (Fig. 15b). Perhaps this is not surprising given the large temperature perturbation and high supersaturation after evaporation of the ice. Using the ECMWF profiles of temperature and pressure gave an almost identical result. This reinforces the hypothesis that in reality the air was close to, but not at, ice saturation. It also further suggests that the temperature perturbation calculated by the gravity wave scheme is reasonable. Of course, this artificial evaporation could not be included in the actual nudged GCM simulations.

While it has been demonstrated that the parameterisation triggers increased formation of high-level cloud, as required, the actual increases in cloud amount that are produced are not as geographically extensive as appear to be required from the observations (e.g. Fig. 9). Figure 16 profiles the difference in model ice amounts between the control and parameterisation version of the model at the timestep of interest. The

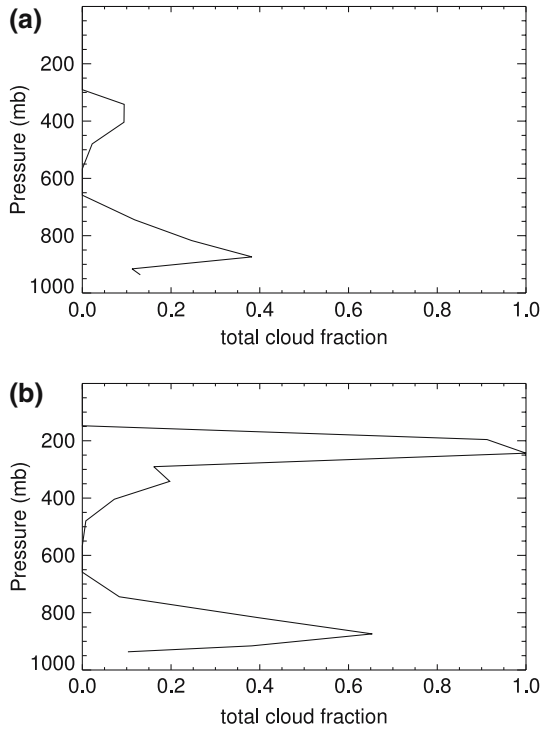

Fig. 15 Offline analysis showing **a** the diagnosed cloud profile without the parameterisation if all of the ice is evaporated and **b** also with all the ice evaporated but with the temperature perturbation due to the sub-grid gravity wave included

difference in the prognostic ice amount carried into the new timestep is shown in (a) with the solid line indicating a large amount of extra ice over the land point, compared with the adjacent gridboxes to the west (dash-dot line) and east (dashed line). After the tracer advection has acted on the ice amounts the difference over the land has decreased while to the east it has increased. From this it can be inferred that the model has advected the ice into the adjacent gridbox. However, after the microphysics scheme has been called, where the extra ice is created over the land, the downstream difference is greatly decreased: most of the extra ice is immediately evaporated. This does not conform with observations such as the cirrus amount in Fig. 9 which suggests that in reality ice is advected away from the mountains for up to 1,000 km. In the Unified Model this would be the equivalent of four gridboxes.

7 Conclusions

We have developed a new parameterisation of sub-grid scale temperature variability due to unresolved orographic gravity waves, based on a linear hydrostatic wave solution that includes phase variations and

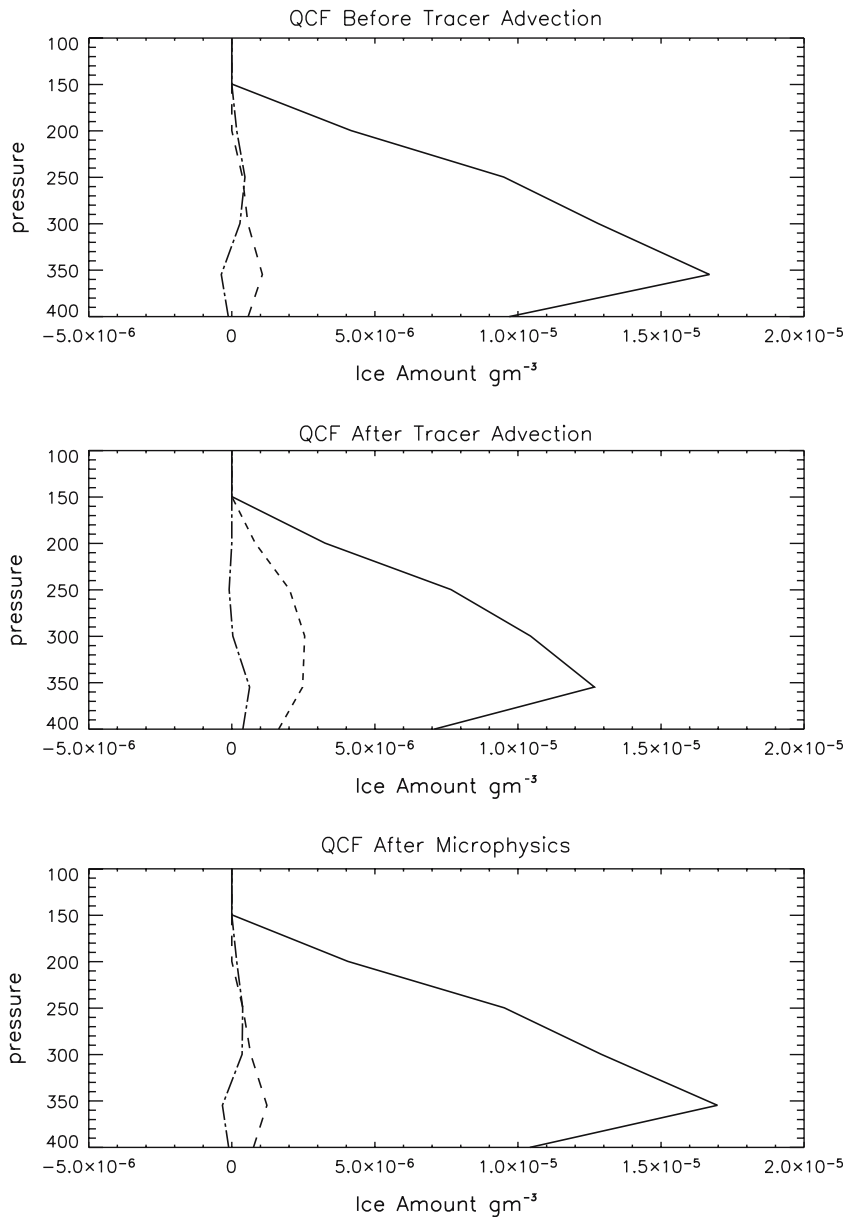

Fig. 16 Profiles of the difference in the ice amount between the parameterisation run and the control run at 0000 GMT on the 1 July 1999 for the southernmost gridbox of New Zealand (*solid line*), the immediately adjacent gridbox to the east (*dashed line*) and the west (dashed-dot line). In **a** the profiles are at the beginning of the model timestep, **b** immediately after ice has been advected by the tracer advection and **c** at the end of the timestep after the microphysics scheme has been called

utilises a directional launch amplitude. It has been shown by comparison with a two-dimensional high resolution model forced by observations that the scheme can reproduce the typical amplitudes and phases of mountain wave oscillations produced by flow over long two-dimensional mountain ranges. For a parameterisation in a GCM, where the 'average' over long time scales is ultimately the most important aspect, the correspondence in amplitude was excellent.

Subsequently, a large orographic cloud generated by flow across the Southern Alps of New Zealand was studied using various satellite imagery and retrieved cloud properties. The synoptic conditions of this situation were recreated by nudging the Unified Model's winds, temperatures and humidities towards those of ERA-40. While generating additional cloud over the mountains in the control simulation, principally through an increase in low cloud, the model did not produce an orographic cloud such as that seen in the observations. The presence of increased high cloud upwind of the mountains compared to the observations made interpretation of the experiment more difficult. When the new sub-grid gravity wave scheme was employed a significant increase in cloud was seen to the east of the South Island. It was shown that more dramatic changes in cloud cover would have occurred if, as suggested by satellite observations, the upper troposphere in the model was free of ice upwind of New Zealand.

The tendency for the model to return rapidly to its original equilibrium restricts the potential of the parameterisation to produce orographic cirrus clouds as large as those identified in observations (e.g. Dean et al. 2005) as being lacking in the Unified Model. It may be necessary to utilise the sub-grid gravity scheme more directly by using it to predict vertical velocities for input into an ice microphysics scheme such as that proposed by Karcher and Lohmann (2002).

Acknowledgments The ISCCP data were obtained from the NASA Langley Research Center Atmospheric Sciences Data Center. The ERA-40 Re-analysis data were obtained from the United Kingdom Met Office through the British Atmospheric Data Centre. This work was partially funded by the NERC thematic programme Clouds Water Vapour and Climate, the Marsden Fund of the Royal Society of New Zealand and the New Zealand Foundation for Research Science and Technology under contract C01X0202.

References

Bacmeister JT, Newman PA, Gray BL, Chan KR (1994) An algorithm for forecasting mountain wave-related turbulence in the stratosphere. Weather Forecast 9:241–253

Broutman D, Rottman JW, Eckermann SD (2004) Ray methods for internal waves in the atmosphere and ocean. Annu Rev Fluid Mech 36:233–253

Butchart N, Knight JR (1999) Estimates of sub-grid temperature perturbations from a gravity wave drag parameterization in a GCM. In: Carslaw KS, Amanatidis GT (eds) Mesoscale processes in the stratosphere—their effects on stratospheric chemistry and microphysics, no. 69 in European Commission air pollution research report

Carslaw KS, Peter T, Bacmeister JT, Eckermann SD (1999) Widespread solid particle formation by mountain waves in the Arctic stratosphere. J Geophys Res 104:1827–1836

Cusack S, Edwards JM, Kershaw R (1999) Estimating the subgrid variance of saturation and its parameterization for use in a GCM cloud scheme. Q J R Meteorol Soc 125:3057–3076

Dean SM, Lawrence BN, Grainger RG, Heuff DN (2005) Orographic cloud in a GCM: the missing cirrus. Clim Dyn 24:771–780

Eckermann SD, Preusse P (1999) Global measurements of stratospheric mountain waves from space. Science 286:1534–1537

Eckermann SD, Gibson-Wilde DE, Bacmeister JT (1998) Gravity wave perturbations of minor constituents: a parcel advection methodology. J Atmos Sci 55:3521–3539

ECMWF (1995) User Guide to ECMWF Products 2.1, European Centre for Medium-Range Weather Forecasting

Feichter J, Lohmann U (1999) Can a relaxation technique be used to validate clouds and sulphur species in a gcm? Q J R Meteorol Soc 125:1277–1294

Fowler LD, Randall DA (1999) Simulation of upper tropospheric clouds with the Colorado State University general circulation model. J Geophys Res 104:6101–6121

Gregory D, Shutts GJ, Mitchell JR (1998) A new gravity-wave drag scheme incorporating anisotropic orography and low level wave breaking: impact upon the climate of the UK Meteorological Office Unified Model. Q J R Meteorol Soc 124:463–493

Höpfner M, Larsen N, Spang R, Luo BP, Ma J, Svendsen SH, Eckermann SD, Knudsen B, Massoli P, Cairo F, Stiller G, v Clarmann T, Fischer H (2005) Mipas detects antarctic stratospheric belt of nat pscs caused by mountain waves. Atmos Chem Phys Discuss 5:10723–10745

Jeuken ABM, Siegmund PC, Heijboer LC, Feichter J, Bengtsson L (1996) On the potential of assimilating meteorological analyses in a global climate model for the purposes of model validation. J Geophys Res 101:16939–16950

Karcher B, Lohmann U (2002) A parameterization of cirrus cloud formation: homogeneous freezing of supercooled aerosols. J Geophys Res 107:ACL4–9,ACL4–10

Leung LR, Ghan S (1995) A subgrid parameterisation of orographic precipitation. Theor Appl Climatol 53:95–118

Leung LR, Ghan S (1998) Parameterising subgrid orographic precipitation and surface cover in climate models. Mon Weather Rev 126:3271–3291

Lindzen RS (1981) Turbulence and stress owing to gravity wave and tidal breakdown. J Geophys Res 86,NO.C10:9707–9714

Lohmann U, Feichter J, Chuang CC, Penner JE (1999) Prediction of the number of cloud droplets in the ECHAM GCM. J Geophys Res 104:9169–9198

Mann GW, Carslaw KS, Chipperfield MP, Davies S, Eckermann SD (2005) Large nat particles and dentrification caused by mountain waves in the arctic stratosphere. J Geophys Res 110

McFarlane NA (1987) The effect of orographically excited gravity wave drag on the general circulation of the lower stratosphere and troposphere. J Atmos Sci 44:1775–1800

Nilson ED, Pirjola L, Kulmala M (2000) The effect of atmospheric waves on aerosol nucleation and size distribution. J Geophys Res 105:19917–19926

Palmer TN, Shutts GJ, Swinbank R (1986) Alleviation of a systematic westerly bias in general circulation and numerical weather prediction models through an orographic gravity wave drag parameterisation. Q J R Meteorol Soc 112:1001–1039

Pope VD, Gallani ML, Rowntree PR, Stratton RA (2000) The impact of new physical parameterizations in the Hadley Centre climate model HadAM3. Clim Dyn 16:123–146

Queney P (1948) The problem of airflow over mountains: a summary of theoretical studies. Bull Am Met Soc 29:16–26

Ridley RN (1991) Observations and numerical modelling of air flows over New Zealand, Ph.D. thesis, Monash University

Tan K, Eckermann SD (2000) Numerical simulations of mountain waves in the middle atmosphere over the southern Andes. In: Siskind DE, Summers ME, Eckermann SD (eds) Atmospheric science across the stratopause. Geophysical Monograph, AGU, Washington pp 123:311–318

Watts PD (1995) Potential use of along track scanning radiometer data for cloud parameter retrieval, no. 2578 in Proc Spie Int Soc Opt Eng

Webster S, Brown AR, Cameron DR, Jones CP (2003) Improvements to the representation of orography in the Met Office Unified Model. Q J R Meteorol Soc 129:1989–2010

Wilson DR, Ballard SP (1999) A microphysically based precipitation scheme for the UK Meteorological Office Unified Model. Q J R Meteorol Soc 125:1607–1636

Wilson D, Gregory D (2003) The behavior of large-scale model cloud schemes under idealized forcing scenarios. Q J R Meteorol Soc 129:967–986

Xu KM, Randall DA (1996) A semiempirical cloudiness parameterization for use in climate models. J Atmos Sci 53:3084–3102